Modulating inflammation in a cutaneous chronic wound model by IL-10 released from collagen–silica nanocomposites via gene delivery

Xiaolin Wang, Thibaud Coradin, Christophe Hélary

Modulating inflammation in a cutaneous chronic wound model by IL-10 released from collagen–silica nanocomposites *via* gene delivery†

Xiaolin Wang, Thibaud Coradin * and Christophe Hélary *

Cutaneous chronic wounds remain a major clinical challenge which requires the development of novel wound dressings. Previously, we showed that collagen–silica nanocomposites consisting of polyethyleneimine (PEI)-DNA complexes associated with silica nanoparticles (SiNP), collagen hydrogel and 3T3 fibroblasts, can work as a local "cell factory". Indeed, the "in-gel" transfection leads to a sustained production and release of biomolecules. Herein, we further explored the possibility for nanocomposites to deliver interleukin-10 (IL-10), a potent anti-inflammatory cytokine, which favors tissue repair. Its anti-inflammatory effect was evaluated in an *in vitro* inflammation model carried out by LPS (lipopolysaccharide) activation of macrophages embedded in collagen gel. The IL-10 synthesis from nanocomposites was detected over one week in the range of 200–400 pg mL^{-1} and reached a maximum at day 5 without any observed cytotoxic effects. PEI_{10}-SiNP outperformed free PEI_{10} and PEI_{25}-SiNP, implying that the introduction of SiNP improved the transfection efficiency of low M_w of PEI. In addition, the structure and mechanical properties of collagen–silica nanocomposites were stable over one week. Subsequently, the ability of nanocomposites to modulate inflammation was tested in a 3D model of inflammation. The decrease of TNF-α and IL-1β gene expression by 20–80% indicated successful inhibition of inflammation by IL-10 released from nanocomposites. Taken together, the nanocomposites are capable of producing effective doses of IL-10 which inhibit the synthesis of pro-inflammatory cytokines and favor the expression of wound healing cytokines. Therefore, the as-constructed 3D gene delivery system represents a promising strategy for the controlled release of therapeutic biomolecules favoring cutaneous wound healing.

1. Introduction

Wound healing is a multi-cellular process which occurs immediately after an injury to restore the integrity of skin.[1] A normal wound healing cascade is composed of overlapping phases including homeostasis, inflammation, proliferation and remodeling. Cutaneous chronic wounds are characterized by a chronic state of inflammation which leads to extracellular matrix breakdown, altered re-epithelialization and impaired neovascularization. The most prevalent chronic wounds in the developed world are venous leg ulcers and diabetic foot ulcers.[2]

Macrophages play a central role in the inflammatory response. They exist in a spectrum of phenotypes,[3] ranging from "classically activated" or "M1," to "alternatively activated" or "M2". The M1 phenotype is characterized by the production of pro-inflammatory cytokines (*e.g.* IL-1β, TNF-α, and IL-6), nitric oxide, proteases and reactive oxygen species for host defense whereas M2 macrophages secrete IL-10, an anti-inflammatory cytokine, ornithine and polyamines, thereby leading to inflammation resolution and tissue restoration.[4] In a normal healing process, transition of macrophages from M1 to M2 is mandatory while in the case of chronic wounds, macrophages are hooked in the M1 phenotype, resulting in severe tissue damage. With the aim of modulating inflammation, IL-10 received particular attention thanks to its potent anti-inflammatory properties. Therefore, IL-10 delivery has been extensively investigated to treat chronic inflammation,[5–8] autoimmune diseases[9] and even cancer.[10]

Traditional protein therapy involving direct injection is largely hampered by rapid diffusion and the short half-life of proteins.[11] For example, the apparent *in vivo* half-life of i.p. injected IL-10 was approximately 2 h in mice.[12] Potas *et al.* fabricated an IL-10 functionalized polycaprolactone (PCL) nanofibrous scaffold for nervous tissue repair.[7] Observation of bio-

Sorbonne Universités, UPMC Univ Paris 06, CNRS, UMR 7574, Laboratoire de Chimie de la Matière Condensée de Paris, F-75005 Paris, France.
E-mail: christophe.helary@upmc.fr

†Electronic supplementary information (ESI) available. See DOI: 10.1039/c7bm01024a

logical effects after 14 days of implantation indicated that the immobilization process permitted a considerable extension of the bioavailability period of the cytokine. However, the preparation of the bioconjugated scaffold involved rather sophisticated chemical modifications. Gene therapy represents an interesting alternative to address the above-mentioned issues. Current strategies for IL-10 production *via* gene delivery predominantly involve viral vectors.[13–15] A few attempts have been made with non-viral vectors such as dendrimers,[16] alginate nanoparticles,[9] poly[α-(4-aminobutyl)-L-glycolic acid] (PAGA)[17] and poly(lactide-*co*-glycolide) (PLGA) microparticles.[18] For example, Jain *et al.* have encapsulated pDNA encoding for IL-10 (pIL-10) in alginate nanoparticles, which were then modified with tuftsin peptide to target macrophages for the treatment of rheumatoid arthritis.[9] This targeting system was shown to significantly reduce inflammation and joint damage.

For the treatment of localized diseases such as cutaneous chronic wounds, scaffold-based delivery systems have received more attention to create favorable microenvironment for tissue regeneration.[19] Moreover, spatio-temporal control over bioactive molecule release can achieve optimal efficacy while averting side effects. Shea's group loaded lentivirus carrying pIL-10 in a porous PLGA scaffold.[20] IL-10 gene delivery was found to decrease leucocyte infiltration in the implanted scaffold by 50% relative to controls. Holladay *et al.* co-delivered stem cells and plasmid IL-10 (pIL-10) in a collagen sponge for the treatment of myocardial infarction.[16] The dendrimer-complexed plasmids were adsorbed on the pre-formed collagen scaffold and stem cells were seeded on top of the sponges. The produced IL-10 downregulated the inflammatory response and thereby improved the survival of the transplanted stem cells. Nevertheless, therapeutic genes were rapidly released without any controlled delivery.

Collagen is the most abundant structural protein in skin. Its natural compatibility with skin tissues, suitability for cell adhesion and growth, and versatility in forms of hydrogels, sponges, films, *etc.* provide ideal platforms for accelerated wound healing in chronic wounds.[21] We have previously shown that collagen-based nanocomposites co-encapsulating pDNA/polyethyleneimine (PEI)/silica particles with fibroblasts represent a promising strategy for the local, controlled and sustained release of proteins of interest.[22] The immobilization of PEI-DNA on silica nanoparticles restricted the mobility of DNA polyplexes and silica nanoparticles within the collagen matrix, thereby largely reducing the exposure of normal tissues to PEI and offering a safe delivery platform of therapeutic value. Using pGLuc (luciferase) as a plasmid model, it was demonstrated that gene expression relies on cell migration within the collagen hydrogel, allowing a progressive cell transfection, followed by the prolonged production of the protein. Herein, we further evaluate the performance of silica–collagen nanocomposites as wound dressings to allow sustained and spatio-temporal release of IL-10 in order to modulate inflammation in an *in vitro* 3D model of inflammation obtained by encapsulation of lipopolysaccharide (LPS)-activated macrophages in a collagen matrix (Fig. 1).

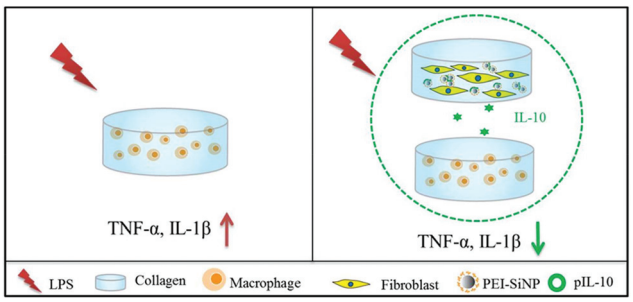

Fig. 1 Scheme of silica-collagen nanocomposites modulating inflammation in an *in vitro* inflammation model. LPS activation results in gene expression of proinflammatory cytokines TNF-α and IL-1β (left panel), which would be inhibited by anti-inflammatory cytokine IL-10 produced and released from gene-loaded silica–collagen nanocomposites (right panel).

2. Materials and methods

2.1. Production of plasmid encoding human IL-10 (phIL-10)

phIL-10 (Origene, USA) is the plasmid pCMV6-XL5 in which the ORF cDNA sequence encoding for human interleukin 10 has been inserted. This plasmid was amplified by using a one shot BL21(DE3) pLysS kit (Invitrogen, Life Technologies), extracted by using a PureLink HiPure Plasmid kit (Invitrogen, Life Technologies), and finally stored in Tris-EDTA buffer at −20 °C.

2.2. phIL-10-PEI and phIL-10-PEI-SiNP complexation

Silica nanoparticles (SiNP), 200 nm in diameter, were prepared and coated with PEI according to our previous procedure.[22] phIL-10 : PEI complexes were prepared at a weight ratio of 1 : 2. pIL-10-PEI-SiNP complexes were prepared at various phIL-10-PEI-SiNP weight ratios. Complex formation was examined by agarose gel electrophoresis (Fig. S1†). Briefly, 2 μL of phIL-10 solution (0.1 μg μL^{-1}) was mixed homogeneously with a total volume of 8 μL of PEI-SiNP (pIL-10 : PEI-SiNP weight ratios of 1 : 1, 1 : 5, 1 : 10, 1 : 20, 1 : 30) suspension or PEI solution (pIL-10 : PEI weight ratio of 1 : 2). The resulting mixtures were left at room temperature for 2 hours to achieve complete complexation, before being loaded into a 0.7% agarose gel with ethidium bromide (0.1 μg mL^{-1}) and running with TAE 1× (Tris acetate EDTA) buffer at 100 V for 40 min. Complex formation was evaluated by observation of the inhibition of DNA migration.

2.3. Mouse fibroblast and macrophage cell culture

Mouse macrophages (RAW264.7 cells) and 3T3 mouse fibroblasts were purchased from Sigma Aldrich. 3T3 mouse fibroblasts were cultured in complete culture medium (DMEM, Glutamax, 10% fetal bovine serum, 1% streptomycin/penicillin) at 37 °C in a moist atmosphere with 5% CO_2. Fibroblasts were detached from the flask using Trypsin EDTA (0.5%) and collected. Macrophages were grown in the same culture medium as 3T3 cells. These cells were harvested by scratching,

centrifuged and suspended in fresh medium. The cell number was evaluated using a standard trypan blue cell counting technique.

2.4. Preparation of silica-collagen nanocomposites

Silica–collagen nanocomposites incorporating 3T3 fibroblasts were prepared according to a previous protocol.[22] Type I collagen solution (2 mg mL^{-1} in 17 mM acetic acid), whole cell culture medium and 0.1 M NaOH solution were kept in ice baths for 1 h before preparation to slow down the gelling kinetics of collagen. 500 μL of the collagen solution was mixed with 245 μL of culture medium by robust vortexing. After addition of 30 μL of 0.1 M NaOH, phIL-10-PEI-SiNP (phIL-10 dose at 5 μg per gel, phIL-10 : PEI-SiNP weight ratio of 1 : 20, total volume of 125 μL) or phIL-10-PEI (phIL-10 : PEI weight ratio of 1 : 2) complexes were added to the mixtures, followed by 100 μL of the 3T3 cell suspension at a density of 1.5×10^6 cells per mL and mixed homogeneously. Then 0.9 mL was sampled from the mixture and deposited into a 24-well plate to avoid air bubbles. The plate was then incubated at room temperature for 15 min for complete gelation of collagen.

2.5. Scanning electron microscopy

Silica–collagen nanocomposites were fixed using 3.63% glutaraldehyde in a cacodylate/saccharose buffer (0.05 M/0.3 M, pH 7.4) for 1 h at 4 °C. Following fixation, samples were washed three times in a cacodylate/saccharose buffer (0.05 M/0.3 M, pH 7.4) and dehydrated through successive increasing concentration ethanol baths from 70% to 100% alcohol. Thereafter, the samples were dried in a critical point dryer and gold sputtered (20 nm) for analysis. The samples were observed with a Hitachi S-3400N SEM operating at 10 kV.

2.6. Rheological measurements

Shear oscillatory measurements on nanocomposites were performed on a rheometer (Anton Paar) equipped with a plane acrylic surface of 24.9 mm diameter. Both base and geometry surfaces were rough in order to avoid sample slipping during measurement. All tests were performed at 37 °C. Mechanical spectra, namely storage, G' and loss, G'' moduli *versus* frequency (1–100 Hz), were recorded at an imposed 1% strain, which corresponded to non-destructive conditions. Before each test, the gap between the base and geometry was chosen when a slight positive normal force was applied on gels during measurement. Samples of all groups of collagen hydrogel were tested at day 2, 5, and 7 ($n = 3$).

2.7. Cell transfection and cell viability

Transfection efficiency of phIL-10-PEI and phIL-10-PEI-SiNP was evaluated both in 2D and 3D configurations by the titration of the hIL-10 protein secreted into the cell culture medium using an ELISA-kit for hIL-10 (Novex, Life Technologies).

To perform cell transfection in 2D, 3T3 mouse fibroblasts were plated at a density of 5×10^4 per well into a 24-well plate. phIL-10-PEI or phIL-10-PEI-SiNP complexes (1 μg DNA per well, with weight ratios of 1 : 2 for PEI and 1 : 20 for PEI-SiNP in a final volume at 25 μL) were added to the cell culture medium. After 4 hours, the supernatant was removed, the well was washed once with PBS (1×) and refreshed with 1 mL medium. The cells were then cultured for another 44 h in complete medium for the expression of hIL-10. Finally, the medium from each well was collected and frozen until analysis with an ELISA test.

To perform cell transfection in 3D, silica–collagen nanocomposites were prepared as described in section 2.4 (5 μg DNA per well, with weight ratios of 1 : 2 for PEI and 1 : 20 for PEI-SiNP in a final volume at 125 μL) and incubated after gelling with 1 mL of fresh medium. The ability of nanocomposites to produce and secrete hIL-10 was analyzed over one week. At day 2, 5 and 7, 500 μL of the culture medium was collected from the wells, frozen and replaced with an equal volume of fresh medium. Control groups were prepared and cultured under the same culture conditions as the experiment groups except for the absence of DNA complexes. Free PEI 25 kDa (PEI_{25}) and 10 kDa (PEI_{10}) were used as positive controls and complexed with DNA at a weight ratio of 1 : 2 before being encapsulated in collagen.

Cell viability was monitored using the Alamar Blue test. For the 2D model, cell culture medium was collected after 2 days and replaced by 200 μL of the Alamar Blue solution (10% in cell culture medium). Cell viability was calculated and reported as a percentage of the control group ($n = 3$). At day 7, cell viability was assessed in the 3D models (nanocomposites) using the same procedure, except that 800 μL water was first added to the collagen gel over 0.5 h at room temperature to extract the Alamar blue solution trapped in the gel and then collected for the absorbance measurements.

2.8. Design of an *in vitro* inflammation model

To establish an *in vitro* model of inflammation, macrophages were encapsulated in collagen and subsequently subjected to lipopolysaccharide (LPS, Sigma-Aldrich) activation to mimic an inflammation state in the wound bed. With this aim, 10^5 RAW264.7 cells were encapsulated in a 1 mg mL^{-1} collagen gel with the volume of 1 ml and cultured for one day prior to LPS activation. LPS at a concentration of 1 μg mL^{-1} was added to macrophage embedded collagen gels for 1 h to induce inflammation in a 3D context. The choice of activation period of 1 h was based on the study of TNF-α gene expression kinetics in a 2D context (Fig. S2†).

To investigate the modulation effect of hIL-10 on the abovementioned inflammation model, macrophage embedded collagen gels were pretreated with hIL-10 containing medium in the range of 0.2–0.8 ng mL^{-1} one hour before LPS activation, and the gels were cultured for 1 h with 1 μg mL^{-1} LPS. Subsequently, collagen was digested with collagenase (1 mg mL^{-1}, pH 7.4) for 15 min at 37 °C, after which macrophages were collected by centrifugation, treated by Trizol (Invitrogen, Carlsbad, CA, USA) and finally stored at −80 °C before RNA extraction. Gene expression of TNF-α was applied as an inflammatory marker and was quantified by qPCR as described in section 2.11.

2.9. Modulatory effect of IL-10 produced from nanocomposites on gene expression of TNF-α, IL-1β and IL-10 in the *in vitro* inflammation model (3D context)

To evaluate the inflammation modulation effect of silica–collagen nanocomposites onto the inflammation model, silica–collagen nanocomposites and collagen gels containing macrophages were first prepared following the protocol presented in sections 2.4 and 2.7, respectively. The nanocomposites were immediately used after their fabrication or after 3 or 5 days in culture. After one day post preparation, macrophage-containing collagen gels were transferred to the same well where the nanocomposites were present and co-cultured with them for a period of 2 days. Two days later, 1 μg mL^{-1} LPS was added to the culture well to induce inflammation. After 1 hour activation, macrophage embedded collagen gels were subjected to collagenase digestion (Sigma) at 2 mg mL^{-1} for 15 min at 37 °C. Subsequently, the macrophages were collected by centrifugation, treated with Trizol (Invitrogen, Carlsbad, CA, USA) and finally stored at −80 °C before RNA extraction. The gene expression of TNF-α, IL-1β and mouse IL-10 was quantified by qPCR as described in section 2.11.

2.10. Total RNA extraction and cDNA synthesis

All the studies were carried out in a designated PCR clean area. RNAs were extracted using the RNeasy mini-kit (Qiagen, France) according to the manufacturer's recommendations. The absorbance ratio of 260/280 nm was used to evaluate the purity of the obtained RNA and the value at 1.9–2.0 was considered as good quality. To eliminate the contamination with genomic DNA, a DNase digestion was performed for 15 min. First-strand cDNA was synthesized at 37 °C by M-MLV reverse transcriptase (Invitrogen, France).

2.11. Measurement of gene expression by real time PCR (Q-PCR)

Real-time quantitative PCR amplifications were carried out in a Light Cycler 480 detection system (Roche, France), using the Light Cycler Fast Start DNA Master plus SYBR Green I kit (Roche, France). The mRNA transcript level of TNF-α, IL-1b and IL-10 was normalized with the housekeeping gene GAPDH because its expression is not modified under our conditions. Cycling conditions were: initial denaturation at 94 °C for 5 min, followed by 40 cycles consisting of a 10 s denaturation at 94 °C, a 15 s annealing at 59 °C and a 15 s elongation at 72 °C. Then, a melting curve was obtained for each sample by increasing the temperature from 59 °C to 97 °C at a rate of 0.11 °C s^{-1}.

Gene expressions of TNF-α, IL-1β and IL-10 were quantified using the absolute quantification method with arbitrary values (n = 4). For this purpose, a standard curve was obtained for each target and reference gene. Primer efficiencies were calculated in each experiment from the standard curve obtained in the same plate as the quantified samples. For each sample, a ratio of target gene/reference gene was calculated and compared with a calibrator point. This calibrator point was the cDNA obtained from the control samples at day 2 (without LPS activation and hIL-10 treatment). The value 1 was given to the mean of ratios for the control samples (n = 4). Arbitrary values were then calculated for each condition by comparison with the value 1, using the ratios. Primer sequences for TNF-α, IL-1 β, IL-10 and GAPDH are presented in Table S1.†

2.12. Statistical analysis

Results are presented as mean ± SD (standard deviation). Statistical significance was assessed using one way analysis of variance (ANOVA) followed by the Tukey (compare all pairs of groups) or Dunnett (compare a control group with other groups) *post hoc* test. The level of significance in all statistical analyses was set at a probability of $P < 0.05$. Prism (GraphPad) software was used for all data analysis.

3. Results and discussion

3.1. SEM characterization

As shown in Fig. 2, the obtained silica–collagen nanocomposites exhibited a macroporous structure formed by collagen fibrils with a diameter around 50 nm. 3T3 fibroblasts were found to be spindle-shaped, suggesting their successful biointegration within the collagen network. Independent of the PEI chain length, phIL-10-PEI-SiNP were found to be small aggregates apparently sticking to the collagen fibrils.

3.2. Rheological measurements

The mechanical properties of 3T3-cellularized collagen hydrogels and nanocomposites were investigated by rheological measurements at day 2, 5 and 7. Storage, G' and loss, G'' moduli were measured *versus* frequency. In each case, G' was *ca*. ten times larger than G'' (Fig. S3†) and both G' and G'' were almost independent of frequency (in the 1–10 Hz range), as common features of physical hydrogels.

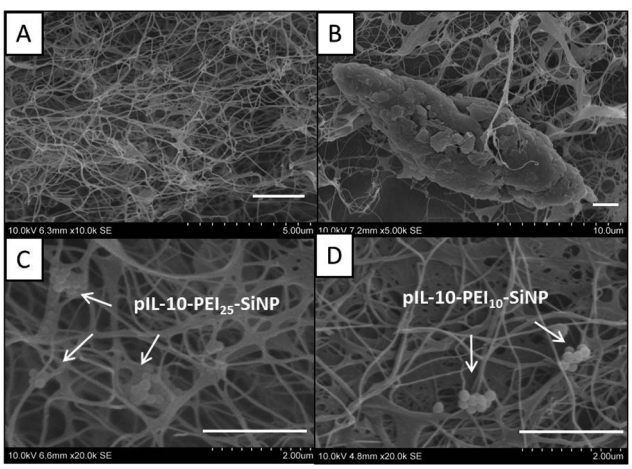

Fig. 2 Structure of silica–collagen nanocomposites observed with SEM at day 5. (A) Collagen matrix, (B) 3T3 fibroblasts, (C) pIL-10-PEI_{25}-SiNP and (D) pIL-10-PEI_{10}-SiNP (scale bar: 2 μm).

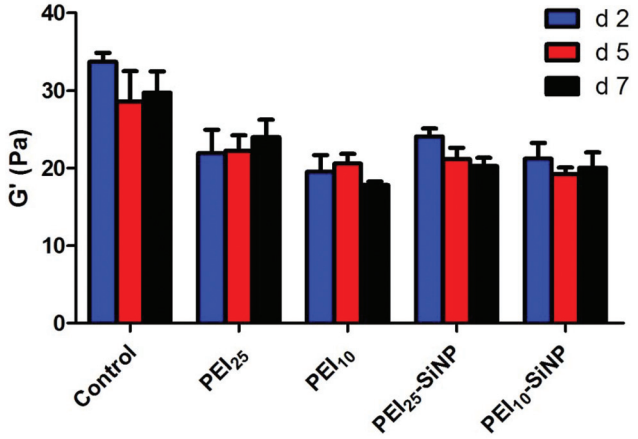

Fig. 3 Storage modulus G' of collagen gels over 1 week.

G' values were averaged at a unique frequency (1 Hz) for each group and are given in Fig. 3. Incorporation of phIL-10-PEI_{25} complexes induced a moderate decrease of G' from *ca.* 30 Pa to *ca.* 20 Pa. A similar small decrease of G' value was measured in the presence of the phIL-10-PEI-SiNP particles, suggesting that they do not have a significant impact on the formation of the hydrogels, as expected from the low introduced concentration (100 μg mL^{-1}). Furthermore no significant difference was observed for all the groups from day 2 to day 7, indicating a stable system over one week of culture.

3.3. Production of hIL-10 by 3T3 fibroblasts transfected in 2D

The quantification of hIL-10 in the culture media evidenced that the PEI-coated silica nanoparticles complexed with phIL-10 were able to transfect 3T3 fibroblasts (Fig. 4). While the highest production of hIL-10 was achieved using PEI_{25} alone, both PEI_{25}-SiNP and PEI_{10}-SiNP carriers showed superior transfection ability compared to PEI_{10} alone. Although these profiles are similar to those obtained using the pGLuc plasmid,[21] the difference in measured transfection efficiency between the free PEI_{25} and PEI_{10}-SiNP is here smaller, the latter achieving 40% of the quantity of hIL-10 produced by 3T3 cells after transfection with the former. In the meantime, it was observed that neither the free polymer nor the PEI-coated particles showed significant cytotoxicity at the low concentrations used (*i.e.* 2 μg mL^{-1} and 20 μg mL^{-1}, respectively) (Fig. S4†). It is worth noting that unlike PEI-coated particles, the free PEI becomes rapidly toxic when the concentration increases (from 10 μg mL^{-1}).

3.4. Production of hIL-10 from SiNP-collagen nanocomposites

The ability of 3T3 cells to produce hIL-10 was then evaluated in a 3D context after the co-encapsulation of cells and PEI or PEI-SiNP complexes within a collagen hydrogel. The synthesis of hIL-10 was detectable from day 2 and lasted over one week regardless of the transfection system used (Fig. 5). However, compared to the 2D situation, increasing the plasmid dose from 1 μg to 5 μg per gel was found necessary in the 3D context to detect a significant hIL-10 production. Actually, cells are not directly in contact with the vectors, and they have to migrate to be transfected. Hence increasing the dose enhances the probability of transfection. These results are in agreement with Fontana *et al.*,[23] who showed that the expression of therapeutic genes from collagen/hyaluronic acid microgels depended on the dose of polyplexes encapsulated within collagen microspheres. Noticeably, while such an increase in plasmid content imposes an increase in the PEI or PEI-SiNP content, these higher doses induce no significant toxic effect on the 3T3 cells (Fig. S5†). Under these conditions, the hIL-10 production reached a maximum at day 5 with concentrations comparable to those obtained under 2D conditions. This delay of synthesis could be attributed to the time for 3T3 cells to migrate within the collagen network and encounter transfection systems. The slight decrease of hIL-10 concentration detected at day 7 in PEI-SiNP systems could be

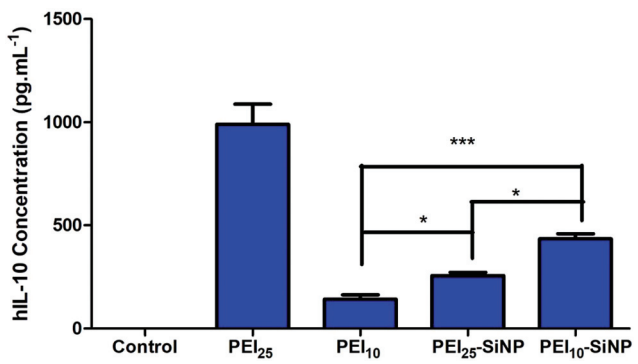

Fig. 4 Transfection of 3T3 mouse fibroblasts after a 4 hour incubation with free or silica-associated PEI complexed with phIL-10 (n = 3). Variance of the IL-10 expression among groups PEI_{10}, PEI_{25}-SiNP, and PEI_{10}-SiNP was determined by one-way ANOVA with the Tukey *post hoc* test (*P < 0.05, **P < 0.01, ***P < 0.001).

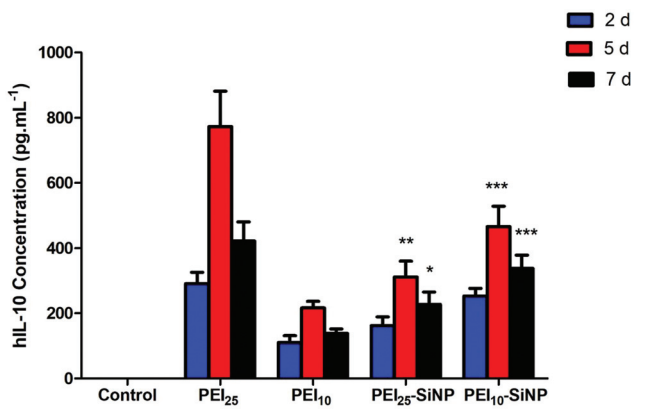

Fig. 5 Production of IL-10 by 3T3 mouse fibroblasts encapsulated within silica-collagen nanocomposites (n = 3). Variance of the IL-10 expression among groups PEI_{10}, PEI_{25}-SiNP, and PEI_{10}-SiNP was determined by one-way ANOVA with the Tukey *post hoc* test (*P < 0.05, **P < 0.01, ***P < 0.001).

due to the IL-10 instability in culture medium.[24] In contrast the drastic decrease of hIL-10 in PEI_{25} systems could be related to the diffusion of soluble form of PEI. Indeed it has been previously shown that only soluble PEIs are able to diffuse through collagen gels.[22]

3.5. Dose dependent effect of hIL-10 on activated macrophages

The activation of collagen-immobilized macrophages by addition of LPS was first checked *via* gene expression of TNF-α, a specific marker of inflammation, and a LPS concentration of 1 μg mL^{-1} was selected as it allowed reaching an expression level after 1 h similar to that obtained under 2D conditions (Fig. S5†). In a second step, the ability of hIL-10 solutions to modulate TNF-α expression in LPS-activated immobilized macrophages was evaluated *via* a dose–response study. As shown in Fig. 6, the highest tested hIL-10 concentration (0.8 ng mL^{-1}) allowed to reduce TNF-α expression by more than 60% compared to the LPS only group, in agreement with the literature.[15]

3.6. Effect of hIL-10 produced from silica–collagen nanocomposites on activated macrophages within an *in vitro* model of inflammation

In our study, plasmid encoding for human IL-10 instead of murine IL-10 was adopted given the fact that the human IL-10 has a comparable biological effect to the murine counterpart on mouse macrophages. Besides, it would also facilitate the further investigation on a set of human cells. Based on this knowledge, we subsequently investigated the possibility to modulate inflammation using hIL-10 proteins released from the above-described cellularized phIL-10-PEI and phIL-10-PEI-SiNP-collagen nanocomposites. In this study, collagen hydrogels containing macrophages were co-cultured with these nanocomposites for a 2-day period after which LPS was added to the medium for 1 h to induce the inflammatory phenotype of macrophages. The inflammation modulation was monitored by quantitative PCR in terms of gene expression in activated macrophages of the pro-inflammatory cytokines, TNF-α and IL-1β and an anti-inflammatory cytokine, IL-10, using non-activated macrophages as the reference. Monitoring these three molecules with different roles and mechanisms of action simultaneously allows for a more detailed following of the M1 to M2 phenotype switch.

As seen in Fig. 7, LPS activation resulted in a significant increase in the production of pro-inflammatory cytokines,

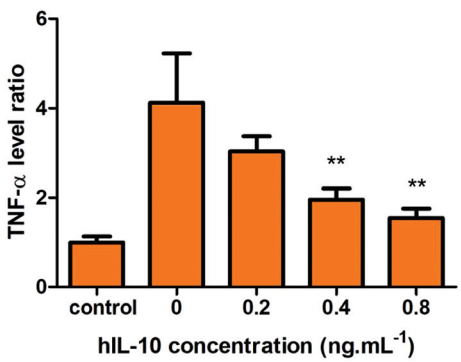

Fig. 6 The gene expression of TNF-α at different IL-10 concentrations with a constant LPS concentration at 1 μg mL^{-1} determined by qPCR and presented in the ratio compared with that of the control group in 3D (n = 3). Variance of the TNF-α expression among IL-10 treated groups was determined by one-way ANOVA with the Tukey *post hoc* test (*P < 0.05, **P < 0.01, ***P < 0.001).

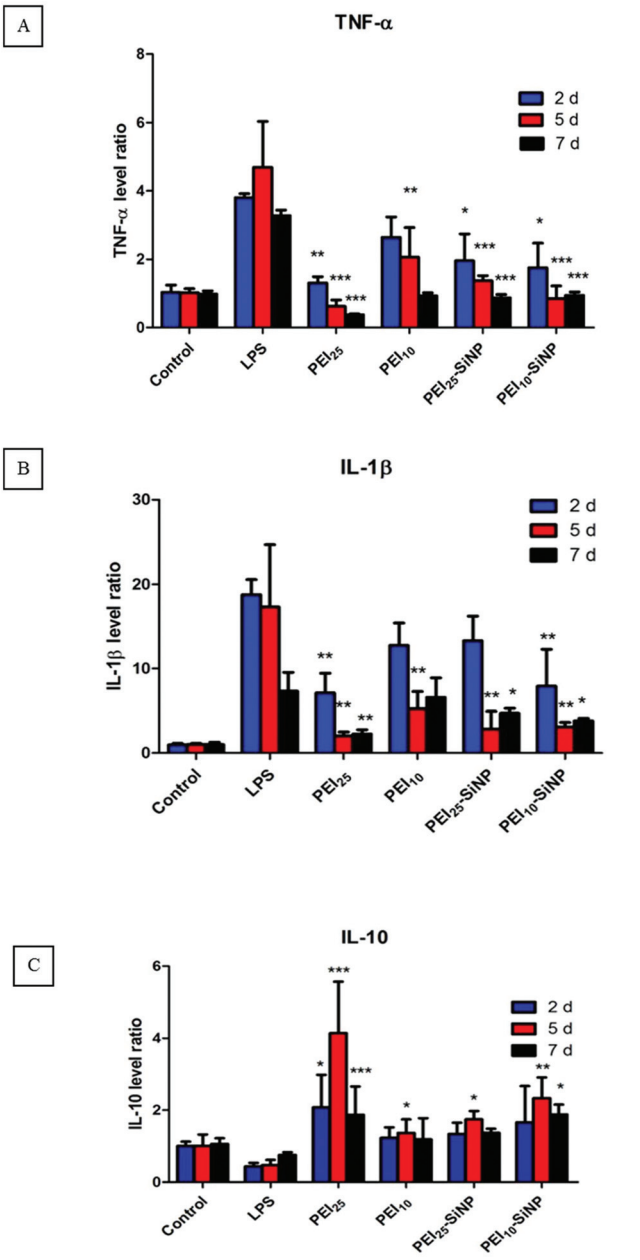

Fig. 7 The gene expression of TNF-α (A), IL-1β (B) and IL-10 (C) at different time points, determined by qPCR and presented in the ratio compared with that of the control group. Variance of the noted cytokine expression level between the LPS only group and those co-cultured with DNA complexes containing hydrogel groups on 2, 5 and 7 d respectively was determined by one-way ANOVA with Dunnett's *post-hoc* test, *P < 0.05, **P < 0.01, ***P < 0.001.

TNF-α (A) and IL-1β (B) and a slight decrease in the expression of IL-10 (C).

The levels of pro-inflammatory cytokines were significantly reduced in the PEI_{25} group over a 1 week observation, down to a level similar to non-activated macrophages. For the PEI_{10} group, significant suppression was only observed on day 5. Regarding IL-10 gene expression, a considerable increase was observed for the PEI_{25} group over 1 week, as high as 4 times that of the non-treated control group on day 5. For the silica–collagen nanocomposites, the decrease of TNF-α and IL-1β expression levels was observed from day 2 while an increase of IL-10 was observed from day 5, signing for a switch from M1 to M2 macrophage phenotype. It is interesting to point out that the efficiency of the different systems varies according to the hIL-10 expression profile measured in the nanocomposites (Fig. 4), *i.e.* PEI_{25} > PEI_{10}-SiNP > PEI_{25}-SiNP > PEI_{10}. This clearly demonstrates that the macrophage response within the collagen hydrogels (*i.e.* in our chronic wound model) is directly related to hIL-10 production by 3T3 fibroblasts encapsulated in the silica–collagen scaffold.

It can be observed that when free hIL-10 was added at a 0.8 ng mL^{-1} concentration to immobilized activated macrophages, the reduction of TNF-α expression was *ca.* 60% after 1 h compared to non-activated cells (Fig. 6). However, a pretreatment for 2 days by nanocomposites releasing a similar hIL-10 concentration resulted in a remarkable reduction of *ca*. 87%. More impressively, nanocomposite-released hIL-10 at a concentration level of 0.4 ng mL^{-1} achieved a reduction of TNF-α production of 83% to be compared with a 53% decrease following 1 h exposure to a hIL-10 solution at the same concentration. This points out that a continuous and sustained hIL-10 production suppresses TNF-α production more robustly than does transient exposure to hIL-10 protein.[15] The main advantage in the utilization of PEI_{10}-SiNP compared with the soluble form of PEI_{25} is the absence of plasmid diffusion outside the nanocomposites. This prevents the undesirable transfections in the wound bed, thus hindering side effects. In addition, PEI_{10}-SiNP is at least 10 times less toxic than PEI_{25}. As a result, it is possible to load 10 times more of nanocomposites. This could permit a higher or a longer effect on chronic wounds.

It is well accepted that the balance of macrophage phenotype plays important roles in the wound healing cascade as M1 fight against infection while M2 promote extracellular matrix (ECM) synthesis and cell proliferation. However, macrophages are prone to switch from M2 to M1 in pathological situations, especially in kidney disease, atherosclerosis and chronic venous ulcers.[4] More generally, macrophages are locked in a M1 phenotype in chronic wounds. Hence, the sustained release of IL-10, a cytokine known to promote the switch between the M1 and M2 macrophage phenotype is of interest for the resolution of inflammation. In addition, the delivery of IL-10 is crucial for wound healing as this cytokine has an effect on the organization of the ECM. Indeed it has been shown that transgenic mice (IL-10 −/−) exhibited impaired scarring with a fragile ECM.[25] So far, biomaterials able to favor the M1 to M2 phenotype switch using IL-10 gene delivery have relied on the preparation of scaffolds containing the gene-loaded vector. To model the *in vivo* situation after implantation, macrophages are seeded on top of the scaffold and are able to infiltrate the matrix. In this case, the gene delivery targets the macrophages and the produced IL-10 can modulate their phenotype.[9,15] Another approach would rely on the release of the vector from the scaffold to the wound bed, with an associated risk of plasmid uncontrolled dissemination.[26] In contrast, our strategy is based on the production and release of hIL-10 by fibroblast cells co-immobilized with the gene carriers within collagen hydrogels. As no contact between the macrophages and the gene vectors is required, the infiltration step is no longer required and the possible occurrence of plasmid dissemination is limited. Moreover, these materials do not need to be implanted but can be used as temporary wound dressings on the skin wound bed.

Silica–collagen nanocomposites exhibit better resistance against degradation than pure collagen hydrogels.[27] However, collagen nanocomposites would be in a hostile environment and could be hydrolyzed by proteases in the case of chronic wounds. One possibility to strengthen the structure would be the crosslinking of nanocomposites to abate degradation. It has been previously shown that EDC/NHS[28] or StarPEG crosslinking[29] was compatible with viability of cells encapsulated within collagen hydrogels. Moreover, crosslinking mode has been proved to have a direct effect on the degradation profiles of collagen mediated by macrophages.[30] Another option would be increase of collagen concentration. We have shown that the concentrated collagen hydrogel exhibited better resistance to *in vivo* degradation as well as improved mechanical properties.[31]

In our model of inflammation, macrophages in collagen gels were found to proliferate in bundles (data not shown) and exhibited good viability over one week (Fig. S6†), although a term of only 2 days was investigated in the current project. As mentioned before, cross-talk among cells play an important role in wound healing. An interesting research orientation would be the co-culture of fibroblasts and macrophages within the same nanocomposite. Indeed, wound healing macrophages (M2 phenotype) could also modulate the fibroblast phenotype to switch from the inflammatory phase to the proliferative one, thereby leading to skin repair.[1,32] Macrophages adjust their behavior in response to subtle changes in the environment, and reversible switches between M1 and M2 were observed.[33] Thus it would be of high interest to challenge the co-cultured hydrogels with different stimulus modes.

Subsequent to the chronic inflammation, bacterial infection can occur. This infection increases inflammation and leads to limb amputation in some cases.[34] The macrophage M1 phenotype is the most effective to combat infection as these cells release reactive oxygen species and have high abilities of phagocytosis. Hence, modulating inflammation when the wound is infected is pointless. We have previously shown that antibiotic-loaded silica nanoparticles could be associated with a collagen hydrogel to form nanocomposites exhibiting antibacterial properties over one week.[27] Combining IL-10 pro-

duction *via* gene delivery and antibiotic release within the same nanocomposites would therefore be of great interest. As the highest production of IL-10 occurs after 5 days, it would set aside the time for released antibiotics to resolve infection before wound healing is promoted.

4. Conclusions

Gene-loaded collagen–silica nanocomposites encapsulating 3T3 fibroblast cells are able to produce effective doses of hIL-10 that inhibit the synthesis of pro-inflammatory cytokines by macrophages immobilized within collagen hydrogels. These cells also progressively secrete IL-10, signing for a switch from the M1 to M2 phenotype. These results are obtained without requiring direct interactions between the gene carriers and target inflammatory cells. These nanocomposites therefore allow for a spatio-temporal control of inflammation: during the first days after the injury, they could slightly modulate the inflammation to permit wound debridement by macrophages and, after some time, the inflammation inhibition would be more effective to switch towards the proliferative phase of tissue repair.

Given the fact that macrophages are highly plastic, more studies are worth carrying out to further verify the capability of silica–collagen nanocomposites in directing and maintaining macrophages to the M2 phenotype under a different stimulus. Feedback of fibroblasts resulting from the macrophage phenotype shift would also be an interesting research orientation to disclose whether the fibroblasts progress to a proliferative phase, which would then lead to successful wound healing.[1,25]

Conflicts of interest

The authors declare no competing financial interest.

References

1 A. J. Singer and R. A. F. Clark, *N. Engl. J. Med.*, 1999, **341**, 738–746.
2 L. I. F. Moura, A. M. A. Dias, E. Carvalho and H. C. de Sousa, *Acta Biomater.*, 2013, **9**, 7093–7114.
3 D. M. Mosser and J. P. Edwards, *Nat. Rev. Immunol.*, 2008, **8**, 958–969.
4 N. Wang, H. Liang and K. Zen, *Front. Immunol.*, 2014, **5**, 614.
5 E. C. Dengler, L. A. Alberti, B. N. Bowman, A. A. Kerwin, J. L. Wilkerson, D. R. Moezzi, E. Limanovich, J. A. Wallace and E. D. Milligan, *J. Neuroinflammation*, 2014, **11**, 92–113.
6 C. A. Jackson, J. Messinger, J. D. Peduzzi, D. C. Ansardi and C. D. Morrow, *Virology*, 2005, **336**, 173–183.
7 J. R. Potas, F. Haque, F. L. Maclean and D. R. Nisbet, *J. Immunol. Methods*, 2015, **420**, 38–49.
8 S. Buff, H. Yu, J. McCall, S. Caldwell, T. Ferkol, T. R. Flotte and I. Virella-Lowell, *Gene Ther.*, 2010, **17**, 567.
9 S. Jain, T.-H. Tran and M. Amiji, *Biomaterials*, 2015, **61**, 162–177.
10 A. A. Book, K. E. Fielding, N. Kundu, M. A. Wilson, A. M. Fulton and J. Laterra, *J. Neuroimmunol.*, 1998, **92**, 50–59.
11 T. Lipiäinen, M. Peltoniemi, S. Sarkhel, T. Yrjönen, H. Vuorela, A. Urtti and A. Juppo, *J. Pharm. Sci.*, 2015, **104**, 307–326.
12 L. Li, J. F. Elliott and T. R. Mosmann, *J. Immunol.*, 1994, **153**, 3967–3978.
13 S. M. Buff, H. Yu, J. N. McCall, S. M. Caldwell, T. W. Ferkol, T. R. Flotte and I. L. Virella-Lowell, *Gene Ther.*, 2010, **17**, 567–576.
14 C.-L. Fu, Y.-H. Chuang, L.-Y. Chau and B.-L. Chiang, *J. Gene Med.*, 2006, **8**, 1393–1399.
15 R. M. Boehler, R. Kuo, S. Shin, A. G. Goodman, M. A. Pilecki, J. N. Leonard and L. D. Shea, *Biotechnol. Bioeng.*, 2014, **111**, 1210–1221.
16 C. A. Holladay, A. M. Duffy, X. Chen, M. V. Sefton, T. D. O'Brien and A. S. Pandit, *Biomaterials*, 2012, **33**, 1303–1314.
17 J. J. Koh, K. S. Ko, M. Lee, S. Han, J. S. Park and S. W. Kim, *Gene Ther.*, 2000, **7**, 2099–2104.
18 E. D. Milligan, S. J. Langer, T. S. Hughes, E. M. Sloane, J. H. Mahoney, B. M. Jekich, S. F. Maier, L. A. Leinwand and L. R. Watkins, *Mol. Ther.*, 2006, **13**, S99–S99.
19 C. Chaudhary and T. Garg, *Crit. Rev. Ther. Drug Carrier Syst.*, 2015, **32**, 277–321.
20 R. M. Gower, R. M. Boehler, S. M. Azarin, C. F. Ricci, J. N. Leonard and L. D. Shea, *Biomaterials*, 2014, **35**, 2024–2031.
21 L. I. Moura, A. M. Dias, E. Carvalho and H. C. de Sousa, *Acta Biomater.*, 2013, **9**, 7093–7114.
22 X. Wang, C. Hélary and T. Coradin, *ACS Appl. Mater. Interfaces*, 2015, **7**, 2503–2511.
23 G. Fontana, A. Srivastava, D. Thomas, P. Lalor, P. Dockery and A. Pandit, *Bioconjugate Chem.*, 2014, **26**, 1297–1306.
24 G. Kenis, C. Teunissen, R. De Jongh, E. Bosmans, H. Steinbusch and M. Maes, *Cytokine*, 2002, **19**, 228–235.
25 A. King, S. Balaji, L. D. Le, T. M. Crombleholme and S. G. Keswani, *Adv. Wound Care*, 2014, **3**, 315–323.
26 C. Cam and T. Segura, *Curr. Opin. Biotechnol.*, 2013, **24**, 855–863.
27 G. S. Alvarez, C. Hélary, A. M. Mebert, X. Wang, T. Coradin and M. F. Desimone, *J. Mater. Chem. B*, 2014, **2**, 4660–4670.
28 L. Calderon, E. Collin, D. Velascobayon, M. Murphy, D. O'Halloran and A. Pandit, *Eur. Cells Mater.*, 2010, **20**, 134.
29 E. C. Collin, S. Grad, D. I. Zeugolis, C. S. Vinatier, J. R. Clouet, J. J. Guicheux, P. Weiss, M. Alini and A. S. Pandit, *Biomaterials*, 2011, **32**, 2862–2870.
30 A. Yahyouche, X. Zhidao, J. T. Czernuszka and A. J. P. Clover, *Acta Biomater.*, 2011, **7**, 278–286.

31 C. Helary, I. Bataille, A. Abed, C. Illoul, A. Anglo, L. Louedec, D. Letourneur, A. Meddahi-Pelle and M. M. Giraud-Guille, *Biomaterials*, 2010, **31**, 481–490.
32 S. K. Brancato and J. E. Albina, *Am. J. Pathol.*, 2011, **178**, 19–25.
33 K. L. Spiller, S. Nassiri, C. E. Witherel, R. R. Anfang, J. Ng, K. R. Nakazawa, T. Yu and G. Vunjak-Novakovic, *Biomaterials*, 2015, **37**, 194–207.
34 G. A. James, E. Swogger, R. Wolcott, E. d. Pulcini, P. Secor, J. Sestrich, J. W. Costerton and P. S. Stewart, *Wound Repair Regen.*, 2008, **16**, 37–44.